Phototroph-heterotroph interactions during growth and long-term starvation across *Prochlorococcus* and *Alteromonas* diversity

Osnat Weissberg*, Dikla Aharonovich* and Daniel Sher

Department of Marine Biology, Leon H. Charney School of Marine Sciences, University of Haifa, Israel

* Dikla Aharonovich and Osnat Weissberg contributed equally to this study

Correspondence: dsher@univ.haifa.ac.il

Running title: *Prochlorococcus-Alteromonas* interactions across diversity

Abstract

Microbial interactions such as those between phytoplankton and bacteria been studied intensively using specific model organisms, due to their potential impact on ecosystems and biogeochemistry. Yet, to what extent interactions differ between closely related organisms, or how these interactions change over time or culture conditions, remains unclear. Here, we characterize the interactions between five strains each of two globally abundant marine microorganisms, *Prochlorococcus* (a phototroph) and *Alteromonas* (a heterotroph), from the first encounter between individual strains and over more than a year of repeated cycles of exponential growth and long-term nitrogen starvation. *Prochlorococcus-Alteromonas* interactions had little effect on traditional growth parameters such as *Prochlorococcus* growth rate, maximal fluorescence or lag phase, affecting primarily the dynamics of culture decline, which we interpret as representing cell mortality and lysis. The shape of the *Prochlorococcus* decline curve and the carrying capacity of the co-cultures were determined by the phototroph and not the heterotroph strains involved. Comparing various mathematical models of culture mortality suggests that *Prochlorococcus* death rate increases over time in mono-cultures but decreases in co-cultures, with cells potentially becoming more resistant to stress. Our results demonstrate intra-species differences in ecologically-relevant co-culture outcomes. These include the recycling efficiency of

N and whether the interactions are mutually synergistic or competitive. They also highlight the information-rich growth and death curves as a useful readout of the interaction phenotype.

Significance Statement

Interactions between phytoplankton and marine bacteria impact global ecosystems and biogeochemistry. Here, we explore how intra-species variability affects the interactions between *Prochlorococcus*, a globally abundant photosynthetic cyanobacetrium and *Alteromonas*, a heterotrophic bacterium that lives off and recycles organic matter. Under nitrogen starvation, *Prochlorococcus* growing alone increasingly accumulate damage and die, whereas in co-culture with *Alteromonas* they become increasingly resilient. The specific *Prochlorococcus* strain had a much larger effect on co-culture behavior than the *Alteromonas* strain, determining whether the interactions are mutually synergistic or potentially competitive. These results show how ecologically relevant outcomes of interactions may vary between closely related microorganisms, and highlight growth and death curves from laboratory (co)-cultures as information-rich views of microbial growth and death.

Keywords: Microbial interactions, growth curves, machine learning, mortality, co-culture, synergism, Weibull.

Introduction

Interactions among microorganisms occur in every known ecosystem (recently reviewed by (1,2)). Detailed studies of the interactions between selected model organisms (often in laboratory co-cultures) have begun to reveal the diversity of molecular mechanisms whereby organisms interact with each other (2–4). However, it is currently unknown to what extent the studied interactions differ between organism pairs, growth stages or environmental conditions. For example, while broad-scale phylogenetic patterns are often observed in microbial interactions, closely related bacteria may differ in the way they interact with other organisms, likely as a result of the significant genetic diversity observed in many microbial clades (e.g. (5,6)). Additionally, the same

56 pair of interacting organisms can synergize or compete depending on the composition of the
57 culture media and the growth stage of (co)-culture (e.g. (7–9)). Finally, both the coarse-grained
58 ecological classification of microbial interactions (e.g. positive/negative) and the high-resolution
59 mechanistic view obtained using advanced physiology and 'omics approaches are difficult to
60 translate into quantitative, predictive models of organismal growth and decline (1,10,11).

61 Here, we explore to what extent intra-clade diversity affects the outcome of microbial
62 interactions, using growth curves as an information-rich view of microbial growth and mortality.
63 Growth curves can be divided into discrete phases (lag, exponential, stationary, decline and long-
64 term stationary phases), and can be used to extract quantitative parameters such as growth rates,
65 lag times, etc. (12,13). An extra layer of more subtle information may exist in the shapes of the
66 growth curves, providing hints of important shifts in the physiology of the growing organisms, as
67 classically demonstrated by Jacques Monod for diauxic growth in *E. coli* (14). Notably, while many
68 studies of bacterial interactions focus on the exponential growth stage or on culture yield at a
69 specific time-point (e.g. (15–17)), fewer studies look at the shape and dynamics of the decline
70 phases, which can provide important hints regarding the effect of interactions on the process of
71 microbial mortality (e.g. (18–20)).

72 Our model organisms are two globally abundant clades of marine bacteria: a cyanobacterial
73 primary producer (*Prochlorococcus*) and a heterotrophic γ-proteobacterium (*Alteromonas*).
74 Interactions between marine phototrophs (phytoplankton, including cyanobacteria) and
75 heterotrophic bacteria have been studied intensively, as phytoplankton are responsible for about
76 one-half of the photosynthesis on Earth (e.g. (21–25)). Thus, phytoplankton-bacteria interactions
77 may strongly affect community structure and function on scales from microns to thousands of
78 kilometers (26,27). Our model primary producer, *Prochlorococcus*, is found throughout the
79 euphotic zone, the sunlit upper portion, of the oligotrophic (nutrient-poor) ocean. There are
80 multiple *Prochlorococcus* clades, broadly partitioned into high-light (HL) and low light (LL) adapted
81 ecotypes, which differ in their photosynthetic parameters and occupy different niches in the
82 ocean (e.g. surface vs deep water, reviewed by (28)). Strains differ also in traits such as the
83 capacity to utilize different forms of inorganic nutrients and organic matter, as well as in their
84 interactions with heterotrophic bacteria and phage. *Alteromonas* is a clade of free-living marine
85 bacteria, which are also partitioned into surface and deep groups (*A. macleodii* and *A.*
86 *mediterranea*, respectively) (29). *Alteromonas* strains also exhibit diverse capabilities to utilize

87 carbohydrates, to acquire iron, and in motility (30). Interactions between individual strains of
88 *Prochlorococcus* and *Alteromonas* have been characterized in some detail (12,27,31–35). While
89 the phenotype and gene expression patterns during interactions vary between strains, this
90 variability has not been explored systematically (12,32,36). Notably, strain- and condition-
91 dependent phytoplankton-heterotroph interactions are observed also in other systems, including
92 *Synechococcus*, a close relative of *Prochlorococcus* (18,37,38), as well as eukaryotic microalgae
93 (e.g. coccolithophores and diatoms, (7–9,39)).

94 We characterized the interactions between five strains each of *Prochlorococcus* and *Alteromonas*,
95 from the first encounter between previously-axenic strains (i.e., grown in mono-culture) and
96 across ~1.2 years of co-culture (25 phototroph-heterotroph combinations, Figure 1A,
97 Supplementary Figure S1). The culturing period spanned multiple cycles of exponential growth,
98 culture decline and long-term nitrogen starvation (33). Nitrogen limitation occurs across wide
99 swaths of the global ocean, and affects a significant fraction of the *Prochlorococcus* diversity
100 (40,41). We focused our analysis on *Prochlorococcus* growth and decline, which is easily measured
101 using bulk culture fluorescence in a non-invasive manner (e.g. (12,42)). Using this dataset of 429
102 growth curves, as well as associated cell counts, we ask: i) How do the interactions between
103 *Prochlorococcus* and *Alteromonas* vary across the diversity of each organisms? ii) Do the
104 interactions change over time (i.e. do the organisms adapt to "living together")? iii) When, during
105 the life-cycle of a *Prochlorococcus* batch culture, do microbial interactions have the largest impact
106 on growth, death, and overall culture carrying capacity, and can this impact be quantified?

107

108 ## Results

109 ### All *Alteromonas* strains support long-term survival of *Prochlorococcus* under N
110 starvation

111 *Prochlorococcus*, and to some extent *Synechococcus*, have previously been shown depend on co-
112 occurring heterotrophic bacteria to survive various types of stress, including nitrogen starvation
113 (33,34,42,43). At the first encounter between previously-axenic *Prochlorococcus* and
114 *Alteromonas* (E1), all co-cultures and axenic controls grew exponentially (Figure 1B, C). However,
115 all axenic cultures showed a rapid and mostly monotonic decrease in fluorescence starting shortly

116 after the cultures stopped growing, reaching levels below the limit of detection after ~20-30 days.
117 None of the axenic *Prochlorococcus* cultures were able to re-grow when transferred into fresh
118 media after 60 days (Figure 1C). In contrast, the decline of co-cultures rapidly slowed, and in some
119 cases was interrupted by an extended "plateau" or second growth stage (Figure 1B). Across
120 multiple experiments, 92% of the co-cultures contained living *Prochlorococcus* cells for at least
121 140 days, meaning that they could be revived by transfer into fresh media. Thus, the ability of
122 *Alteromonas* to support long-term N starvation in *Prochlorococcus* was conserved in all analyzed
123 strains.

124 It has previously been shown that *Prochlorococcus* MIT9313 is initially inhibited by co-culture with
125 *Alteromonas* HOT1A3, while *Prochlorococcus* MED4 is not (12,32). This "delayed growth"
126 phenotype was observed here too, was specific to MIT9313 (not observed in other
127 *Prochlorococcus* strains) and occurred with all *Alteromonas* strains tested (Figure 1D). MIT9313
128 belongs to the low-light adapted clade IV (LLIV), which are relatively distant from other
129 *Prochlorococcus* strains and differ from them in multiple physiological aspects including the
130 structure of their cell wall (44), the use of different (and nitrogen-containing) compatible solutes
131 (45) and the production of multiple peptide secondary metabolites (lanthipeptides,(46,47)). LLIV
132 cells also have larger genomes, and are predicted to take up a higher diversity of organic
133 compounds such as sugars and amino acids (48). It is intriguing that this strain, which has higher
134 predicted metabolic and regulatory flexibilities (49), is the only one initially inhibited in co-culture
135 with *Alteromonas*.

136

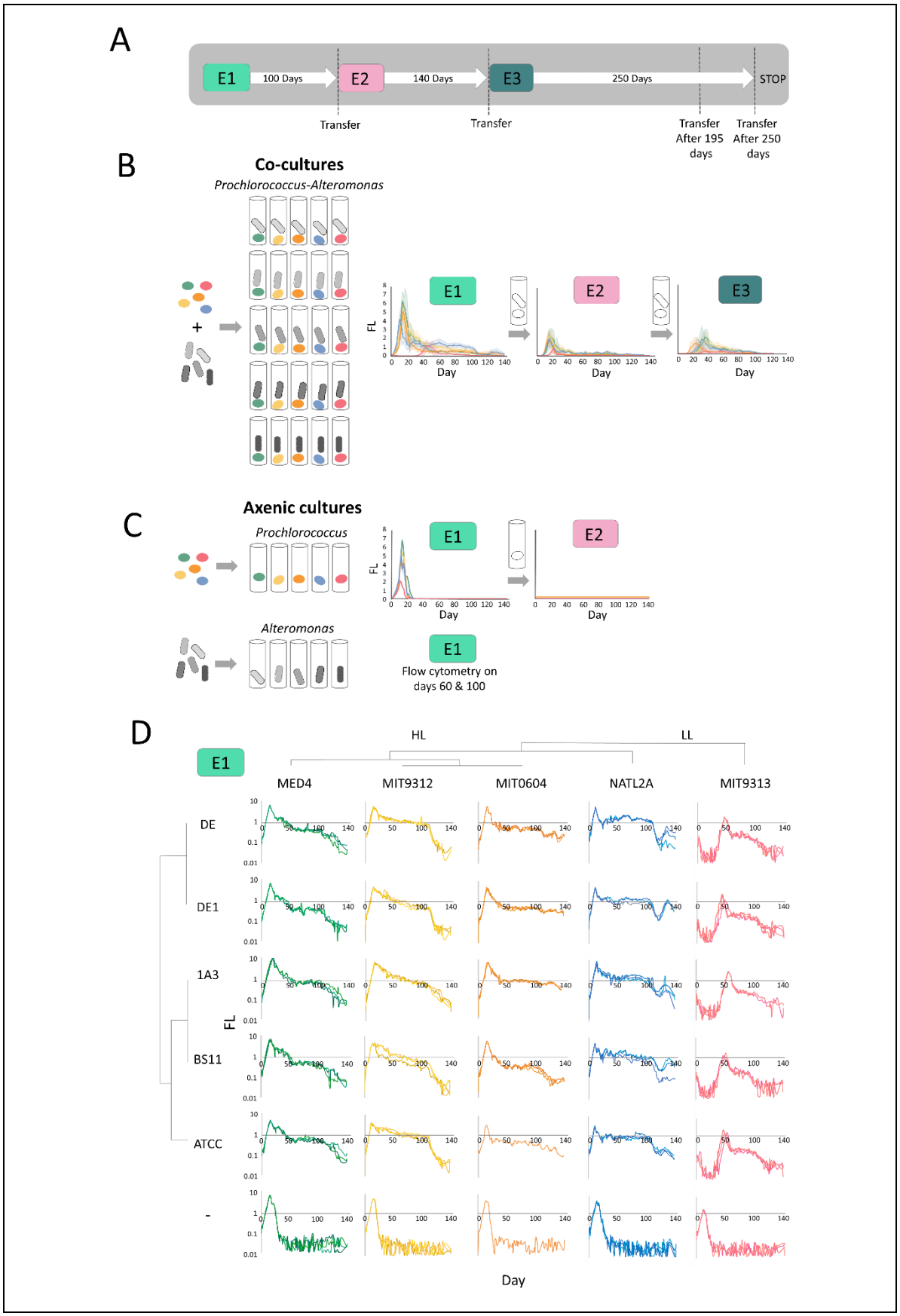
A
E1
100 Days
E2
140 Days
E3
250 Days
STOP
Transfer
Transfer
Transfer After 195 days
Transfer After 250 days
B
Co-cultures
Prochlorococcus-Alteromonas
E1
E2
E3
FL
Day
C
Axenic cultures
Prochlorococcus
Alteromonas
E1
E2
Flow cytometry on days 60 & 100
D
HL
LL
E1
MED4
MIT9312
MIT0604
NATL2A
MIT9313
DE
DE1
1A3
BS11
ATCC
-
FL
Day

Figure 1: Experimental designs and overview of the dynamics of *Prochlorococcus-Alteromonas* co-cultures from first encounter and over multiple transfers. A. Schematic illustration of the experimental design. 1 ml from Experiment E1 was transferred into 20 ml fresh media after 100 days, starting experiment E2. Experiment E2 was similarly transferred into fresh media after 140 days, starting experiment E3. Additional experiments replicating these transfers are described in Supplementary figure S1. B. Overview of the growth curves of the 25 *Prochlorococcus-Alteromonas* co-cultures over three transfers spanning ~1.2 years (E1, E2 and E3). Results show mean + standard error from biological triplicates, colored by *Prochlorococcus* strain as in panel D. C. Axenic *Prochlorococcus* grew exponentially in E1 but failed to grow when transferred into fresh media after 60 days. Axenic *Alteromonas* cultures were counted after 60 and 100 days, as their growth cannot be monitored sensitively and non-invasively using fluorescence (optical density is low at these cell numbers). D. High reproducibility and strain-specific dynamics of the initial contact between *Prochlorococcus* and *Alteromonas* strains (E1). Three biological replicates for each mono-culture and co-culture are shown. Note that the Y axis is linear in panels B, C and logarithmic in panel D.

Differences in co-culture phenotype are related to *Prochlorococcus* and not *Alteromonas* strains and occur primarily during the decline stage

While co-culture with all *Alteromonas* strains had a major effect on *Prochlorococcus* viability during long-term starvation, there was no significant effect of co-culture on traditional metrics of growth such as maximal growth rate, maximal fluorescence and lag phase (with the exception of the previously-described inhibition of MIT9313, Figure 2A,B,C). However, a visual inspection of the growth curves in Figure 1D suggested subtle yet consistent differences in the shape of the growth curve, and especially the decline phase, between the different *Prochlorococcus* strains in the co-cultures. To test this, we used the growth curves as input for a Principal Component Analysis (PCA), revealing that the growth curves from each *Prochlorococcus* strain clustered together, regardless of which *Alteromonas* strain they were co-cultured with (Figure 2D). The growth curves of all high-light adapted strains (MED4, MIT9312 and MIT0604) were relatively similar, the low-light I strain NATL2A was somewhat distinct, and the low-light IV strain MIT9313

152 was a clear outlier (Figure 1D), consistent with this strain being the only one initially inhibited in
153 all co-cultures. Random Forest Classification (a supervised machine learning algorithm) supported
154 the observation that the growth curve shapes were affected more by the *Prochlorococcus* rather
155 than *Alteromonas* strains, and also confirmed the visual observation that most of the features
156 differentiating between *Prochlorococcus* strains occurred during culture decline (Supplementary
157 Figure S2, Supplementary Text S1). Thus, co-culture with *Alteromonas* affects the decline stage of
158 *Prochlorococcus* in co-culture in a way that differs between *Prochlorococcus* but not *Alteromonas*
159 strains.

160 We next asked whether the phenotypes of interaction, which were observed when high cell
161 densities of *Prochlorococcus* and *Alteromonas* interacted for the first time (E1), were maintained
162 after the cells had grown together in co culture for extended periods. We therefore continued to
163 transfer the co-cultures into fresh media over multiple additional transfers, performed 40-200
164 days after the initial inoculations. In total, FL measurements are available for a cumulative period
165 of 380 days which the cells spent in co-culture (Figure 1A, Supplementary Figure S1). The ability
166 of *Prochlorococcus* to survive long-term N starvation, the clustering of the growth curves by
167 *Prochlorococcus* but not *Alteromonas* strains, and the results of the Random Forest Classification,
168 were all reproduced in subsequent transfers (Figure 1B, Supplementary figures S2, S3, S4,
169 Supplementary Text S2). These observations are thus robust to the cumulative time the organisms
170 have been interacting and the cell densities of both organisms when transferred to new media
171 (see below).

172

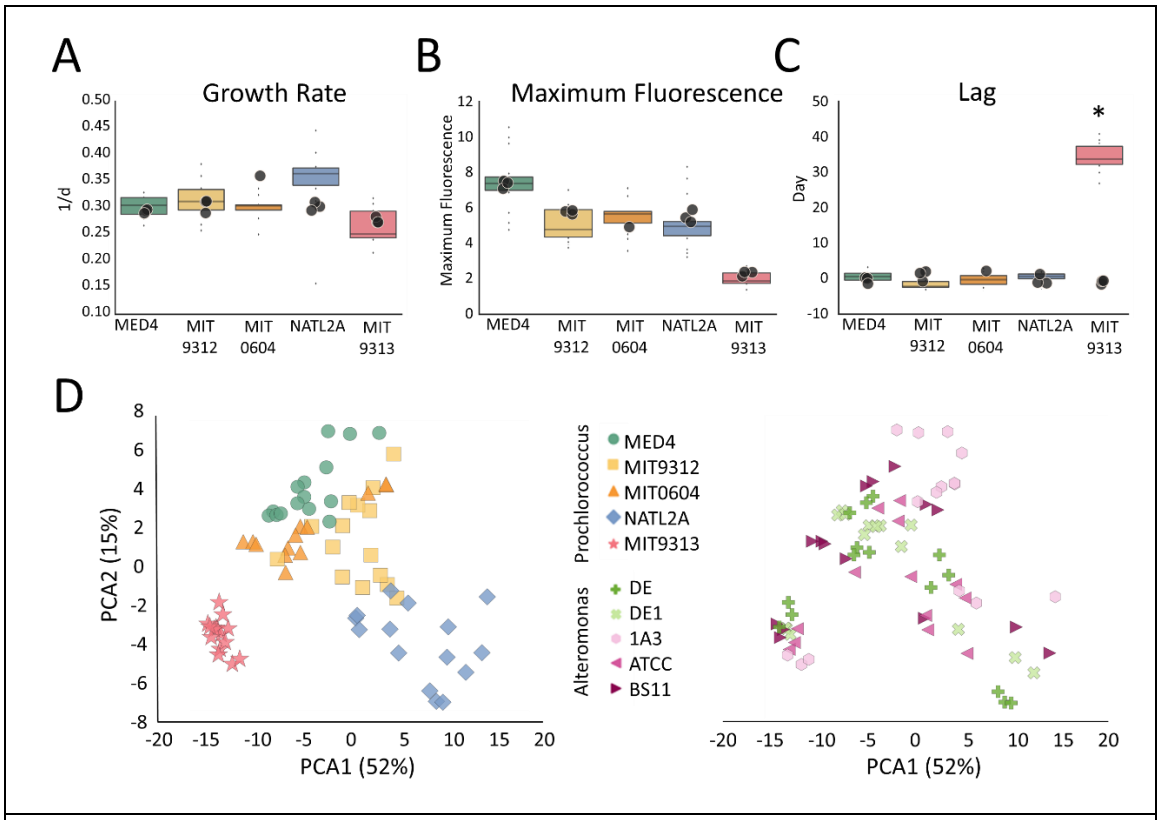

Figure 2: Growth analysis and principal component analysis (PCA) of the growth curves from all co-cultures during 140 days of E1. A. Growth rate, Maximum fluorescence and Lag phase during E1. Box-plots represent mean and 75th percentile of co-cultures, circles represent measurements of individual cultures of the axenic controls. The only significant difference between axenic and co-cultures is in the length of the lag phase for MIT9313 (Bonferroni corrected ANOVA, $p < 0.001$. B. PCA ordination colored by *Prochlorococcus* (left) and by *Alteromonas* (right) strains. The growth curves cluster by *Prochlorococcus* strain (Adonis test, $F(4,68) = 42.3$, $p = 0.001$) and only marginally by *Alteromonas* strain (Adonis test, $F(4,68) = 2.29$, $p = 0.017$)

173

174

175 **Differences in the carrying capacity suggest different modes of interaction**

176 While *Alteromonas* clearly support *Prochlorococcus*, by enabling it to survive long-term N
177 starvation, is the reciprocal interaction also synergistic? Do *Prochlorococcus* enhance the growth
178 of *Alteromonas*, and does the interaction affect the overall carrying capacity of the system,
179 defined here as the ability to efficiently utilize the limiting resource (nitrogen)? To answer these

180 questions, we used the flow cytometry cell counts of *Prochlorococcus* and *Alteromonas* on days
181 60, 100 and 140 to infer the nitrogen (N) biomass of each population grown alone or in co-culture
182 (Figure 3A, Supplementary Table S1, see supplementary text S3 for the calculations and caveats).

183 The overall carrying capacity of the system was higher than the axenic *Alteromonas* cultures,
184 and much higher than the axenic *Prochlorococcus* (Figure 3B). On day 60, the mean carrying
185 capacity of the co-cultures was 2-3 times higher than that of the Axenic *Alteromonas* (69±35
186 compared with 32±22 µmol N/L), suggesting that the heterotroph benefited from carbon fixed
187 by the phototrophic *Prochlorococcus* partner. Indeed, most of this cellular N was found in the
188 *Alteromonas* cells (76±13%). The ability of axenic *Alteromonas* to survive in the absence of
189 organic matter from *Prochlorococcus* is not surprising, as an *Alteromonas* strain distantly related
190 to the ones studied here, AltSIO, can utilize a large fraction of the labile organic material found
191 in natural seawater used to make the growth media (50). In contrast, in axenic *Prochlorococcus*
192 cultures only a small fraction of N in the system was found in cell biomass (~0.01 µmol N/L). This
193 likely reflects the inability of all *Prochlorococcus* strains to recycle organic nitrogen lost due to
194 exudation or cell lysis (Figure 3B).

195 However, mutual synergism was not observed across all strain combinations. While some
196 *Prochlorococcus* strains (MED4, MIT0604, and NATL2A) supported significantly higher
197 *Alteromonas* N biomass compared to the axenic control (log2FC 1.3±0.6), co-cultures with
198 MIT9312 and MIT9313 resulted in similar or lower *Alteromonas* biomass (log2FC -0.2±0.9) (Figure
199 3C). Therefore, on day 60, some of the interactions were mutually synergistic whereas in other
200 cases *Prochlorococcus* do not support *Alteromonas* and may even compete with it. Notably, the
201 two "non-mutually-synergistic" *Prochlorococcus* strains belong to different ecotypes but were
202 isolated from the same drop of water from the Gulf Stream (51). In all co-cultures the
203 *Prochlorococcus* population benefited from the presence of *Alteromonas* (log2FC 10±4).

204 In contrast to day 60, after 100 days essentially all of the interactions were mutually synergistic,
205 with *Alteromonas* supporting the growth of all *Prochlorococcus* strains (log2FC 10±1) and
206 *Prochlorococcus* increasing the *Alteromonas* biomass in all strains with the exception of BS11
207 (log2FC 3±1.5) (figure 3C). This suggests that the mode of interaction (synergist vs competition)
208 may change temporally during the extended period of N starvation.

209 On day 140 the carrying capacity of the co-cultures declined further (only 1% of the N was in
210 biomass). This suggests that the system is not in steady state, with a slow yet constant reduction
211 in carrying capacity. We speculate that this is driven by the loss of bioavailable N from the system
212 (i.e., most of the nitrogen is in a recalcitrant form that cannot be utilized by either partner). This
213 is further supported by the observation that while the co-cultures after 140 days were still alive
214 and could be transferred to new media. In a subsequent experiment, only 16/30 cultures could
215 be transferred after 195 days, and only 3/75 cultures could be transferred after 250 days
216 (Supplementary Figure S5). Notably, MIT0604 (HLII) was the strain most likely to survive transfer
217 after these extended periods and was also the most abundant *Prochlorococcus* strain after 140
218 days (1.46±1 µmol N/L MIT0604 biomass vs 0.26±0.56 µmol N/L for all other strains). While we
219 do not currently have an explanation for the higher survival of this strain, it is noteworthy that it
220 is the only strain to utilize nitrate (52).

221

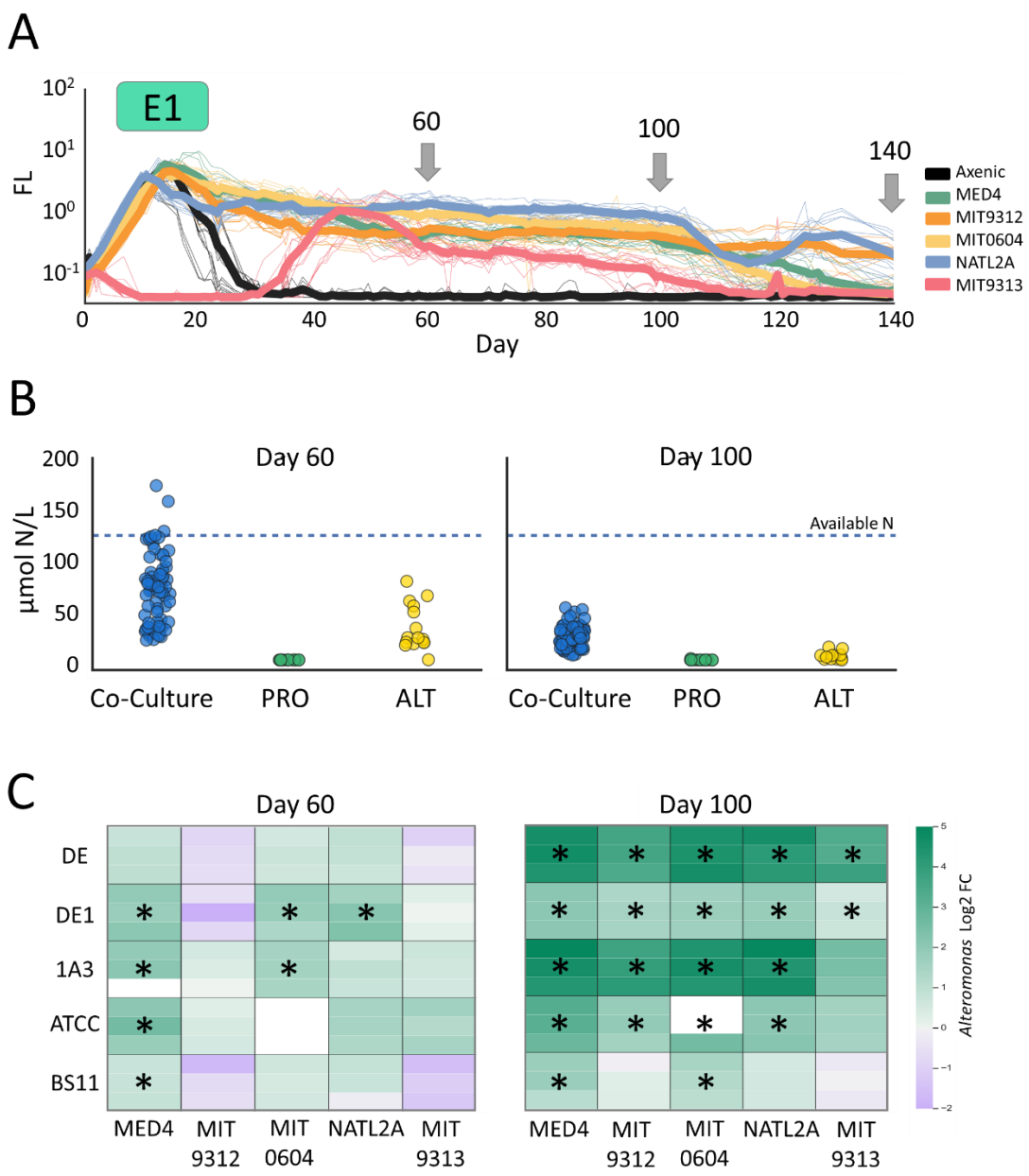

Figure 3: Carrying capacity and type of interactions. A. Growth curves of experiment E1, arrows showing the days where cell numbers were counted by flow cytometry (see also Supplementary Table S1). Axenic curves shown are from all *Prochlorococcus* strains. B. Total calculated N biomass of the cultures in E1 on days 60 and 100 in µmol N/L. Dashed line indicates total available N in co-cultures. C. Log2 Fold Change (FC) of *Alteromonas* N biomass relative to axenic *Alteromonas* controls on days 60 and 100. Asterisks indicate statistically significant FC (Bonferroni corrected ANOVA $p < 0.05$). ALT: *Alteromonas* PRO: *Prochlorococcus*

222

223 **Modeling the effect of co-culture on *Prochlorococcus* mortality**

224 Given that the most striking effect of co-culture was on the decline phase of the co-cultures, we
225 asked whether we could quantify and model the effect of *Alteromonas* on *Prochlorococcus*
226 mortality. Importantly, while the growth of bacteria has been extensively studied and modelled,
227 the decline of bacterial cultures is much less studied, and mortality is rarely represented in
228 ecological or biogeochemical models of microbial dynamics (53). Bacterial mortality has, however,
229 often been modelled in the context of food safety and genome evolution, using either mechanistic
230 or descriptive approaches (53–57). We chose to focus on four of these previously-described
231 models which are relatively simple and have a clear biological interpretation (Table 1). The
232 Exponential model is the simplest and most commonly used one , where a constant portion of the
233 population dies over time (58). The Bi-exponential model is slightly more complex, representing
234 two separate subpopulations in the community, each with its own death rate (55). The Weibull
235 model is probabilistic, modeling a heterogeneous population with a diverse stress tolerance
236 (53,59), finally, the Harmonic model employs a quadratic rate of decline which is often associated
237 with predator-prey interactions or cellular encounter rates (58). When fitting each of these
238 models to the decline phase of the growth curves, the Weibull model stands out as it has a low
239 error for both axenic and co-cultures (Table 1) as well as in consequent transfers (Supplementary
240 Table 1, the biexponential model is a better fit for the co-cultures but does not represent well the
241 axenic ones). Based on the Weibull model, and assuming that culture fluorescence is related to
242 the number of non-lysed cells in the media, axenic *Prochlorococcus* cells die more than ten-fold
243 faster than cells in co-culture (2-decimal reduction time, td_2, is 12.58 ± 3.85 days for axenic
244 cultures and 316 ± 337 days for co-cultures).

245

246

247

248

249

250

251 **Table 1: Mathematical description and biological interpretation of four models used to describe**

252 **bacterial mortality**

Mathematical model[1]	**Derivative**	**# Params**[2]	**Physiological Interpretation**	**Axenic RMSE** [3] **(n=13)**	**Co-culture RMSE (n=343)**	**Reference**
Exponential $X = X_0\, e^{-a\,t}$	$\frac{dX}{dt} = -aX$	1	Constant ratio of the population dies in each time point	0.26 ± 0.11	0.29 ± 0.21	(58)
Bi-Exponential $X = X_0(f\, e^{-a_1\,t} + (1-f)\, e^{-a_2\,t})$	$\frac{dX}{dt} = -f a_1 X_1 - (1-f)\, a_2 X_2$	3	Two subpopulations with different persistence under stress and death rates	0.26 ± 0.11	0.16 ± 0.12	(55)
Harmonic $X = X_0\, \frac{1}{1+a\,t}$	$\frac{dX}{dt} = -a\, X^2$	1	Quadratic mortality rate – dependence on cell-cell encounters	0.50 ± 0.19	0.19 ± 0.13	(58)
Weibull $X = X_0\, e^{-\frac{t^n}{a}}$	$\frac{dX}{dt} = -c\, t^{n-1} X *$	2	Probabilistic model with a heterogeneous distribution of stress tolerance	0.14 ± 0.08	0.18 ± 0.11	(59)

[1] In the mathematical models, *t* stands for time since the beginning of culture decline, *X* and X_0 are the current and initial cell numbers respectively, and the rest of the variables are model parameters (a, f, a_1, a_2, n)

[2] # Params – number of free parameters

[3] RMSE - Root Mean Square Error. Supplementary Table S2 shows also the Bayesian Information Criterion (BIC), which is less intuitive but takes into account also the number of model parameters.

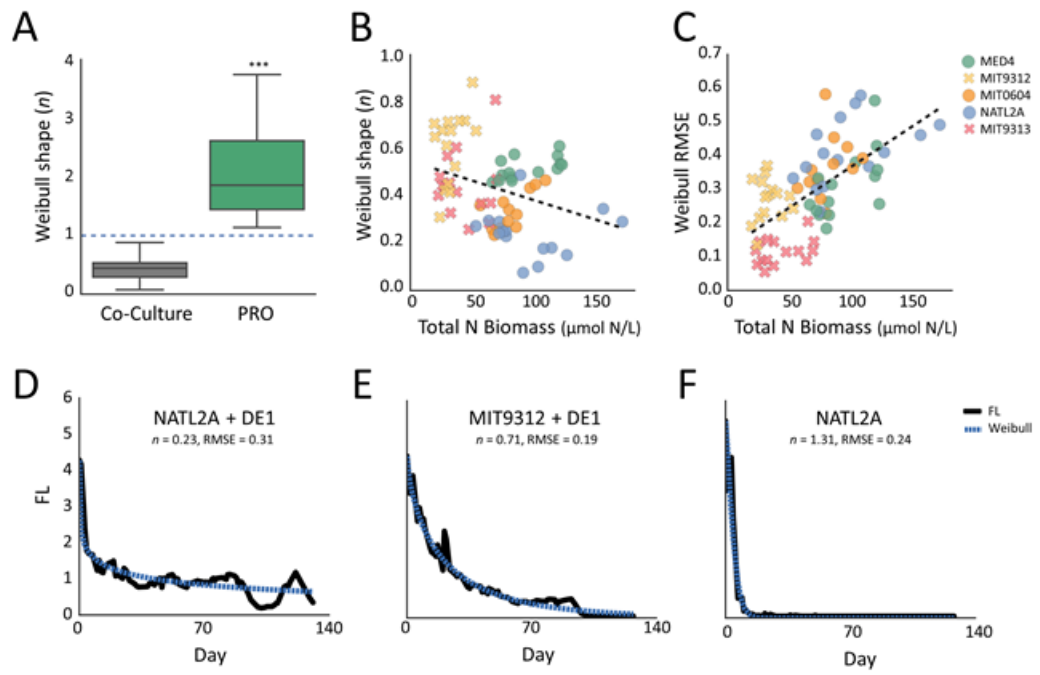

Figure 4: Weibull modeling of long-term starvation. A. Weibull shape (*n*) in Axenic *Prochlorococcus* (PRO) and in Co-cultures. In all axenic samples $n > 1$, in most co-cultures $n < 1$ (students t-test, $p < 0.001$). B. Scatter plot showing the reverse correlation between the total N biomass of the co-cultures on day 60 and Weibull shape (*n*). Pearson r = -0.33, p=5e-3. Circles represent co-cultures with mutual synergistic interactions (i.e. *Prochlorococcus* strains MED4, MIT0604 and NATL2A), X represent potential competitive interactions (strains MIT9312, MIT9313). C. Scatter plot showing the correlation between the total N biomass of the co-cultures on day 60 and Weibull root mean square error (RMSE). Pearson r = 0.64, $p < 0.001$. For the correlations with total N biomass on day 100 see Supplementary Figure S6. D-F. Weibull model fit for selected decline curves. D. Mutually synergistic co-culture of *Prochlorococcus* NATL2A and *Alteromonas* DE1. E. Potentially competitive co-culture of *Prochlorococcus* MIT9312 and *Alteromonas* DE1. F. Axenic *Prochlorococcus* NATL2A

253

254 In the Weibull model, the 'shape parameter' (n) represents the change over time in the
255 susceptibility of the bacterial community to stress. A shape parameter above one represents an
256 increasing probability that cells will die as time increases (e.g. due to the accumulation of
257 damage), whereas a shape parameter below one suggests that, as the culture declines, the cells
258 become more resistant to damage. Axenic cultures have high mean shape value of 2.1 ± 0.9,

259 suggesting an accumulation of cell damage leading to increasing death rate (Figure 4A). In
260 contrast, the mean shape value of co-cultures is significantly lower and below 1 (0.4 ± 0.2, student
261 t-test, $p < 0.001$), suggesting that during N starvation in co-culture the *Prochlorococcus* cells are
262 acclimating over time to the nutrient stress conditions.

263 While the molecular and physiological mechanisms of *Prochlorococcus* adaptation are currently
264 unclear, the Weibull shape parameter decreases as the total N in cellular biomass increases,
265 suggesting that the *Prochlorococcus* acclimation process is related to the ability to recycle N
266 between the specific *Prochlorococcus* and *Alteromonas* strains in co-culture (Figure 4B). Thus, the
267 rate of acclimation is higher in the co-cultures supporting high N biomass and mutually synergistic
268 interaction (NATL2A, MED4 and MIT0604) compared to MIT9312 and MIT9313, where
269 *Alteromonas* do not gain from the interaction (0.36±0.14 vs 0.52±0.16, t-test $p < 0.001$).

270 While the Weibull model is useful in quantifying mortality rates and raising the hypothesis that
271 *Prochlorococcus* cells are acclimating to starvation over time, none of the tested models was able
272 to fully capture the intricate dynamics of culture decline (Figure 4C, D). In most mutually
273 synergistic co-cultures involving *Prochlorococcus* strains NATL2A, MED4 and MIT0604, culture
274 decline was not monotonic, and was interrupted by additional growth phases about 40-50 and
275 100 days after the cultures started declining (Figure 4D). These latter growth phases were mostly
276 absent in co-cultures with MIT9312 and MIT9313 (RMSE 0.2±0.1 vs 0.36±0.1 in the other strains,
277 t-test $p < 0.001$). The correlation between N biomass and the secondary growth phases (i.e.,
278 higher deviation from simple Weibull model, Figure 4C) suggest that these phases may also be
279 related to the ability of the interacting partners to recycle N through mutually-beneficial
280 metabolic interactions.

281

282 Conclusions and Future Prospects

283 Elucidating the mechanisms of microbial interactions requires well-characterized model systems.
284 However, extending the insights from such models across the diversity of organisms and
285 environmental conditions remains challenging. Our results from the highly-simplified system of
286 multiple *Prochlorococcus* and *Alteromonas* strains provide an important step towards this goal.
287 Using the rich information on interaction phenotypes present in the growth and decline curves,
288 we identify conserved and strain-specific facets of these interactions. Despite the genetic diversity

289 across the *Alteromonas* strains studied (30), it was primarily the identity of the *Prochlorococcus*
290 strain that determined the interaction phenotype. This manifests in the growth and decline rates,
291 in the shape of the curve (primarily the decline phase), in the amount of N retained in biomass
292 and in whether the co-cultures are mutually synergistic or, potentially, competitive.

293 Under our laboratory conditions, it is likely that the combined response of both interacting
294 partners to nitrogen starvation underlies the dynamics of the long-term co-cultures, although
295 other stressors such as the increase in osmolarity/salinity or the accumulation of waste products
296 cannot be ruled out (18,34,60). This response is dynamic, as illustrated by the reproducible
297 deviations of the fluorescence curves from the monotonic decline predicted by all models tested
298 ("second growth" stages, Figure 4). Three different (non-mutually-exclusive) processes may
299 underlie these dynamics. Firstly, it is likely that one or both organisms modify their physiology or
300 metabolism over time, for example through the activation of stringent responses, utilization of N
301 or C storage pools, rewiring of metabolism to utilize available N sources or activation of
302 mechanisms such as extracellular enzymes allowing the cells to access previously unusable
303 substrates (e.g. (61,62)). Secondly, it is possible that there are "invisible" ecological dynamics
304 underlying the observed fluorescence curves, for example cyclic changes in the abundance of
305 *Alteromonas* cells. Under such a scenario, rapid *Prochlorococcus* mortality could produce an
306 increase in *Alteromonas* abundance, resulting in degradation and remineralization of dead
307 *Prochlorococcus* biomass and the release of resources that can drive subsequent *Prochlorococcus*
308 growth. Finally, both *Prochlorococcus* and *Alteromonas* populations may be evolving, for example
309 through emergence of genetically-distinct populations better adapted to nutrient starvation
310 (reminiscent of the GASP phenotype described in *E. coli* and other bacteria (63)).

311 Why is it the identity of the primary producer (*Prochlorococcus*) rather than the heterotrophic
312 "recycler" (*Alteromonas*) that determines the outcome of the co-culture? *A-priori*, it was
313 reasonable to assume that the co-culture phenotype would be affected by the differences
314 between the *Alteromonas* strains in their ability to degrade and utilize polysaccharides and a
315 variety of other organic molecule (30,64). We speculate that the increased growth of *Alteromonas*
316 in the co-cultures compared to the axenic ones is fueled primarily by the availability of major
317 biomass components released by *Prochlorococcus* as they die, such as proteins, amino acids and
318 nucleotides. Such common macromolecules do not require highly specialized metabolic processes
319 to degrade and utilize, and hence can be utilized by all of the *Alteromonas* strains (65). It is

320 possible that the differences between *Alteromonas* strains may manifest when more complex
321 macromolecules are available, e.g. from plant material, or when all of the "easy to digest" (labile)
322 organic matter has been utilized and only complex macromolecules remain (66). These conditions
323 may not have been met in our experiments. Similarly, we currently do not know why some
324 *Prochlorococcus* strains support a mutually-synergistic interaction with *Alteromonas* relatively
325 early during the long-term N starvation (day 60) whereas other strains do not, and why at a later
326 stage (day 100) almost all interactions are mutually beneficial. We could not identify any
327 metabolic traits (11) clearly differentiating MIT9313 and MIT9312 (the "competitive" strains) from
328 the others, suggesting more subtle differences exist between the *Prochlorococcus* strains in the
329 organic matter they produce or in their response to N starvation (e.g. (67,68)).

330 Our results identify patterns in the interactions between clades of abundant marine phototrophs
331 and heterotrophs, under conditions where nutrients are scarce, and their availability likely
332 depends on recycling between phototrophs and heterotrophs. Whether or not such mechanisms
333 may be physiologically relevant in the oligotrophic ocean, much of which is N-stressed (40),
334 remains to be tested (conditions in laboratory batch cultures are very different from those in the
335 nutrient-poor ocean). It is, however, noteworthy that the high heterotroph/phototroph biomass
336 ratio observed during long-term N starvation here and in other studies (18) is similar to that of
337 much of the open oligotrophic ocean (e.g. (69)) and references therein). Furthermore,
338 *Alteromonas* may allow *Prochlorococcus* to adapt to light starvation (42) and to the presence of
339 ROS (e.g. (70)), other stressors that can be encountered in the open ocean. However, the
340 supportive role of *Alteromonas* cannot be taken for granted, as it also depends on culture
341 conditions, for example CO_2 concentrations (27).

342 Finally, the co-cultures did not reach a steady state, and did not represent a closed system. Thus,
343 processes not represented in these simplified laboratory co-cultures, are necessary to explain the
344 long-term stability over decades of *Prochlorococcus* in the oceans (71). Such processes could
345 include multi-organism interactions, as natural communities are much more complex than the
346 laboratory co-cultures, as well as oceanographic processes such as nutrient injection through
347 deep mixing. More generally, cell mortality is intimately linked with the amount and type of
348 recycled organic matter, yet the rate of mortality in natural communities is highly unconstrained
349 (72). Hence, better representation of mortality in mathematical models (e.g. the use of
350 appropriate mortality formulations) is likely important for understanding biogeochemical cycles

351 (72). This study is a reminder that bacterial growth curves represent an information-rich
352 representation of the life and death of cells, which can be mined to identify potential physiological
353 changes of ecological relevance.

354

355 Materials and Methods

356 Strains and experiment set up

357 Axenic *Prochlorococcus* strains MED4 (HLI), MIT9312 (HLII), MIT0604 (HLII), NATL2A (LLI) and
358 MIT9313 (LLIV) were maintained under constant cold while light (27 µmole photons m^{-2} s^{-1}) at
359 22ºC (12,73). We used Pro99 media that was modified by reducing the concentration of NH_4 from
360 800µm to 100µm (Pro99-LowN), resulting in *Prochlorococcus* entering stationary stage due to the
361 depletion of available inorganic N (74). *Alteromonas* strains HOT1A3, Black sea 11, ATCC27126,
362 AltDE1 and AltDE were maintained in ProMM media (43). Prior to the experiment, the axenicity
363 of the *Prochlorococcus* cultures was tested by inoculating 1 ml culture into 15 ml ProMM (73). At
364 the start of each co-culture experiment, *Alteromonas* cells from stationary-stage cultures (24-72
365 hour old) were centrifuged (10 minutes, room temperature, 10,000g), the growth media
366 decanted, and the cells re-suspended in Pro99-LowN. The *Prochlorococcus* cultures (growing
367 exponentially) and the re-suspended *Alteromonas* cells were then counted using BD FACSCanto™
368 II Flow Cytometry Analyzer Systems (BD Biosciences). For each co-culture, $1x10^6$ *Prochlorococcus*
369 cells mixed with $1x10^7$ *Alteromonas* cells. For mono-cultures, $1x10^6$ and $1x10^7$ were added for
370 *Prochlorococcus* and *Alteromonas*, respectively. The experiment was performed using triplicate
371 20ml cultures in borosilicate test tubes (2.5cm diameter, 15cm length).

372

373 Fluorescence and Flow cytometry

374 Bulk chlorophyll fluorescence (FL) (ex440; em680) was measured almost daily using a
375 Fluorescence Spectrophotometer (Cary Eclipse, Varian). Samples for flow cytometry were taken
376 after 60, 100 and 140 days of experiment E1, fixed with glutaraldehyde (0.125% final
377 concentration), incubated in the dark for 10 min and stored in -80 °C until analysis. 2 µm diameter
378 fluorescent beads (Polysciences, Warminster, PA, USA) were added as an internal standard. Data
379 was acquired and processed with FlowJo software. Flow cytometry was performed unstained to

count *Prochlorococcus* cells followed by staining with SYBR Green I (Molecular Probes/ ThermoFisher) to count *Alteromonas* cells.

Growth rate

Growth was computed - by solving the equation:

$$N_t = N_0 \, e^{\mu(t-L)}$$

Where N_t represents the number of cells at time *t*, N_0 is the initial number of cells, μ is the growth rate, and *L* is the growth lag. The LAN transformed equation was used to compute growth rate:

$$\ln(N_t) = \ln(N_0) + \mu(t - L)$$

Linear regression was run on the growth phase, predicting $\ln(N_t)$ based on time *t* with $R^2 > 0.9$. The growth rate μ is the regression coefficient.

Fit to Decline models

The following functions were used to fit against the measured fluorescence:

Exponential: $FL_t = FL_{max} \, e^{-a(t-t_{max})}$

Bi-exponential: $FL_t = FL_{\max}(f \, e^{-a_1(t-t_{max})} + (1-f) \, e^{-a_2 \, (t-t_{max})})$

Harmonic: $FL_t = FL_{\max} \frac{1}{1+a\,t}$

Weibull: $FL_t = FL_{\max} \, e^{-a\,t^n}$

Where FL_t is the Fluorescence measured at time *t*, FL_{max} is the maximum fluorescence measured, t_{max} is the time when the fluorescence was highest, and *a, a1, a2, n, f* are the model parameters estimated by the fitting function.

The decline function was fit against each growth curve via curve_fit() function from scipy package (1.3.0), using the parameters: method='dogbox', loss='soft_l1', f_scale=0.1. Each model was fit using random initial parameter values and the initial values of 0.5 per parameter, and the fit with the lowest RSME selected. Goodness of fit was measures using root mean square error (RMSE).

404 In the Weibull model the time needed to reduce the population by *d* factors of 10 (t_{d2}) was
405 estimated as in (59), using the formula:

406 $$t_d = a\,(-ln(10^{-d})^{\frac{1}{n}})$$

407 **Random Forest Classification**

408 To detect difference in the curve pattern and not timing specific differences, the curves were
409 aligned such that max growth point are at time zero, and time points from 10 days prior to max
410 growth to 80 days after were selected. Since the specific measurement time points were different
411 in different experiments and samples, rolling average was used to get mean fluorescence per day,
412 and interpolation used to fill in missing measurements. The Fluorescence measurements were
413 standardized via standard scalar by subtracting the mean and scaling to unit variance of each
414 feature. Random Forest model was run in 10x cross validation to classify the curves by
415 *Prochlorococcus* and by *Alteromonas* strains. To find the most significant days in *Prochlorococcus*
416 classification, the model was built 30 times and the mean importance of all features (i.e.,
417 measurement days) calculated. Data preprocessing was done by pandas (0.25.0). Scaling and
418 model fitting using sklearn (0.21.2).

419 **PCA ordination**

420 PCA ordination was run on the growth curves. The fluorescence measurements were standardized
421 via standard scalar by subtracting the mean and scaling to unit variance of each feature.
422 Ordination was computed via principal component analysis (PCA). Data preprocessing was done
423 by pandas (0.25.0). Scaling and PCA was done using sklearn (0.21.2).

424 **Statistics**

425 Statistics were computed using the statsmodels package in python. Multi test correction was done
426 by t_test_pairwise() using Bonferroni correction. Permanova analysis by adonis2 from R vegan
427 package (R 3.61, vegan 2.5-7).

428

429

430

Acknowledgements

We thank Sher lab members and especially Natalie Andrawes for help in fluorescence measurements and Daniel Segrè, Hans-Peter Grossart, Zhen Wu and Tal Luzzatto Knaan for critical reading of the manuscript. This work was supported by the Human Frontiers Science Program (grant RGP0020/2016, to DS) and the U.S.-Israel Binational Science Foundation (BSF) - U.S. National Science Foundation (NSF) program in Oceanography (grant 1635070/2016532, to DS). The funders had no role in study design, data collection and analysis, decision to publish, or preparation of the manuscript.

Competing Interests

The authors declare no competing financial interests

References

1. Gralka M, Szabo R, Stocker R, Cordero OX. Trophic Interactions and the Drivers of Microbial Community Assembly. Curr Biol [Internet]. 2020;30(19):R1176–88. Available from: https://doi.org/10.1016/j.cub.2020.08.007
2. Fritts RK, McCully AL, McKinlay JB. Extracellular Metabolism Sets the Table for Microbial Cross-Feeding. Microbiol Mol Biol Rev. 2021;85(1).
3. Weisskopf L, Schulz S, Garbeva P. Microbial volatile organic compounds in intra-kingdom and inter-kingdom interactions. Nat Rev Microbiol [Internet]. 2021;19(6):391–404. Available from: http://dx.doi.org/10.1038/s41579-020-00508-1
4. Harrington V, Lau L, Seddu K, Suez J. Ecology and Medicine Converge at the Microbiome-Host. mSystems [Internet]. 2021;6(4):4–8. Available from: https://doi.org/10.1128/mSystems .00756-21
5. Long RA, Azam F. Microscale patchiness of bacterioplankton assemblage richness in seawater. Aquat Microb Ecol. 2001;26(2):103–13.
6. Cordero OX, Wildschutte H, Kirkup B, Proehl S, Ngo L, Hussain F, et al. Ecological Populations of BacteriaAct as Socially Cohesive Units ofAntibiotic Production and Resistance. Science [Internet]. 2012;337(September):1228–31. Available from: http://www.sciencemag.org/content/337/6099/1228.full.pdf%5Cnhttp://www.ncbi.nlm.nih.gov/pubmed/22955834
7. Grossart HP, Simon M. Interactions of planktonic algae and bacteria: Effects on algal growth and organic matter dynamics. Aquat Microb Ecol. 2007;47(2):163–76.
8. Segev E, Wyche TP, Kim KH, Petersen J, Ellebrandt C, Vlamakis H, et al. Dynamic metabolic exchange governs a marine algal-bacterial interaction. Elife.

466 2016;5(NOVEMBER2016):1–28.
467 9. Seyedsayamdost MR, Case RJ, Kolter R, Clardy J. The Jekyll-and-Hyde chemistry of
468 phaeobacter gallaeciensis. Nat Chem. 2011;3(4):331–5.
469 10. Antoniewicz MR. A guide to deciphering microbial interactions and metabolic fluxes in
470 microbiome communities. Curr Opin Biotechnol [Internet]. 2020;64:230–7. Available
471 from: https://doi.org/10.1016/j.copbio.2020.07.001
472 11. Zoccarato L, Sher D, Miki T, Segrè D, Grossart H-P. A comparative whole-genome
473 approach identifies bacterial traits for marine microbial interactions. Commun Biol.
474 2022;5(1):1–13.
475 12. Sher D, Thompson JW, Kashtan N, Croal L, Chisholm SW. Response of *Prochlorococcus*
476 ecotypes to co-culture with diverse marine bacteria. ISME J. 2011;5(7):1125–32.
477 13. Warringer J, Anevski D, Liu B, Blomberg A. Chemogenetic fingerprinting by analysis of
478 cellular growth dynamics. BMC Chem Biol. 2008;8:1–10.
479 14. Monod J. The growth of bacterial cultures. Annu Rev M. 1949;3(Xl):371–94.
480 15. Foster KR, Bell T. Competition, not cooperation, dominates interactions among culturable
481 microbial species. Curr Biol [Internet]. 2012;22(19):1845–50. Available from:
482 http://dx.doi.org/10.1016/j.cub.2012.08.005
483 16. Pacheco AR, Osborne ML, Segrè D. Non-additive microbial community responses to
484 environmental complexity. Nat Commun [Internet]. 2021;12(1):1–11. Available from:
485 http://dx.doi.org/10.1038/s41467-021-22426-3
486 17. Vetsigian K, Jajoo R, Kishony R. Structure and evolution of streptomyces interaction
487 networks in soil and in silico. PLoS Biol. 2011;9(10).
488 18. Christie-Oleza JA, Sousoni D, Lloyd M, Armengaud J, Scanlan DJ. Nutrient recycling
489 facilitates long-term stability of marine microbial phototroph-heterotroph interactions.
490 Nat Microbiol [Internet]. 2017;2(June). Available from:
491 http://dx.doi.org/10.1038/nmicrobiol.2017.100
492 19. Ratzke C, Gore J. Modifying and reacting to the environmental pH drives bacterial
493 interactions. Modifying React to Environ pH can drive Bact Interact. 2017;136838.
494 20. Grossart HP. Interactions between marine bacteria and axenic diatoms (*Cylindrotheca*
495 *fusiformis*, *Nitzschia laevis*, and *Thalassiosira weissflogii*) incubated under various
496 conditions in the lab. Aquat Microb Ecol. 1999;19(1):1–11.
497 21. Field CB, Behrenfeld MJ, Randerson JT, Falkowski P. Primary production of the biosphere:
498 Integrating terrestrial and oceanic components. Science (80-). 1998;281(5374):237–40.
499 22. Cole JJ. Interaction between bacteria and alge in aquatic ecosystems. Ann Rev Ecol Syst.
500 1982;13:291–314.
501 23. Seymour JR, Amin SA, Raina JB, Stocker R. Zooming in on the phycosphere: The ecological
502 interface for phytoplankton-bacteria relationships. Nat Microbiol. 2017;2(May).
503 24. Ramanan R, Kim BH, Cho DH, Oh HM, Kim HS. Algae-bacteria interactions: Evolution,
504 ecology and emerging applications. Biotechnol Adv [Internet]. 2016;34(1):14–29.
505 Available from: http://dx.doi.org/10.1016/j.biotechadv.2015.12.003
506 25. Cirri E, Pohnert G. Algae−bacteria interactions that balance the planktonic microbiome.
507 New Phytol. 2019;223(1):100–6.
508 26. Morris JJ, Lenski RE, Zinser ER. The black queen hypothesis: Evolution of dependencies
509 through adaptive gene loss. MBio. 2012;3(2):1–7.
510 27. Hennon GM, Morris JJ, Haley ST, Zinser ER, Durrant AR, Entwistle E, et al. The impact of
511 elevated CO 2 on *Prochlorococcus* and microbial interactions with â € helper' bacterium
512 *Alteromonas*. ISME J [Internet]. 2018;12(2):520–31. Available from:
513 http://dx.doi.org/10.1038/ismej.2017.189

514 28. Biller SJ, Berube PM, Lindell D, Chisholm SW. *Prochlorococcus*: The structure and function
515 of collective diversity. Nat Rev Microbiol. 2015;13(1):13–27.
516 29. López-Pérez M, Rodriguez-Valera F. Pangenome evolution in themarine bacterium
517 *Alteromonas*. Genome Biol Evol. 2016;8(5):1556–70.
518 30. Koch H, Germscheid N, Freese HM, Noriega-Ortega B, Lücking D, Berger M, et al.
519 Genomic, metabolic and phenotypic variability shapes ecological differentiation and
520 intraspecies interactions of *Alteromonas macleodii*. Sci Rep. 2020;10(1):1–14.
521 31. Hou S, López-Pérez M, Pfreundt U, Belkin N, Stüber K, Huettel B, et al. Benefit from
522 decline: The primary transcriptome of *Alteromonas macleodii* str. Te101 during
523 *Trichodesmium* demise. ISME J [Internet]. 2018;12(4):981–96. Available from:
524 http://dx.doi.org/10.1038/s41396-017-0034-4
525 32. Aharonovich D, Sher D. Transcriptional response of *Prochlorococcus* to co-culture with a
526 marine *Alteromonas*: Differences between strains and the involvement of putative
527 infochemicals. ISME J. 2016;10(12):2892–906.
528 33. Roth-Rosenberg D, Aharonovich D, Luzzatto-Knaan T, Vogts A, Zoccarato L, Eigemann F,
529 et al. *Prochlorococcus* cells rely on microbial interactions rather than on chlorotic resting
530 stages to survive long-term nutrient starvation. MBio. 2020;11(4):1–13.
531 34. Morris JJ, Johnson ZI, Szul MJ, Keller M, Zinser ER. Dependence of the cyanobacterium
532 *Prochlorococcus* on hydrogen peroxide scavenging microbes for growth at the ocean's
533 surface. PLoS One. 2011;6(2).
534 35. Diner RE, Schwenck SM, McCrow JP, Zheng H, Allen AE. Genetic manipulation of
535 competition for nitrate between heterotrophic bacteria and diatoms. Front Microbiol.
536 2016;7(JUN).
537 36. Biller SJ, Coe A, Chisholm SW. Torn apart and reunited: Impact of a heterotroph on the
538 transcriptome of *Prochlorococcus*. ISME J. 2016;10(12):2831–43.
539 37. Zheng Q, Wang Y, Lu J, Lin W, Chen F, Jiao N. Metagenomic and metaproteomic insights
540 into photoautotrophic and heterotrophic interactions in a *Synechococcus* culture. MBio.
541 2020;11(1).
542 38. Calfee BC, Glasgo LD, Zinser ER. *Prochlorococcus* Exudate Stimulates Heterotrophic
543 Bacterial Competition with Rival Phytoplankton for Available Nitrogen . MBio.
544 2022;13(1).
545 39. Amin SA, Hmelo LR, Van Tol HM, Durham BP, Carlson LT, Heal KR, et al. Interaction and
546 signalling between a cosmopolitan phytoplankton and associated bacteria. Nature.
547 2015;522(7554):98–101.
548 40. Ustick LJ, Larkin AA, Garcia CA, Garcia NS, Brock ML, Lee JA, et al. Metagenomic analysis
549 reveals global-scale patterns of ocean nutrient limitation. Science (80-).
550 2021;372(6539):287–91.
551 41. Saito MA, McIlvin MR, Moran DM, Goepfert TJ, DiTullio GR, Post AF, et al. Multiple
552 nutrient stresses at intersecting Pacific Ocean biomes detected by protein biomarkers.
553 Science (80-). 2014;345(6201):1173–7.
554 42. Coe A, Ghizzoni J, LeGault K, Biller S, Roggensack SE, Chisholm SW. Survival of
555 *Prochlorococcus* in extended darkness. Limnol Oceanogr. 2016;61(4):1375–88.
556 43. Morris JJ, Kirkegaard R, Szul MJ, Johnson ZI, Zinser ER. Facilitation of robust growth of
557 *Prochlorococcus* colonies and dilute liquid cultures by "helper" heterotrophic bacteria.
558 Appl Environ Microbiol. 2008;74(14):4530–4.
559 44. Ting CS, Hsieh C, Sundararaman S, Mannella C, Marko M. Cryo-electron tomography
560 reveals the comparative three-dimensional architecture of *Prochlorococcus*, a globally
561 important marine cyanobacterium. J Bacteriol. 2007;189(12):4485–93.

45. Klähn S, Steglich C, Hess WR, Hagemann M. Glucosylglycerate: A secondary compatible solute common to marine cyanobacteria from nitrogen-poor environments. Environ Microbiol. 2010;12(1):83–94.
46. Cubillos-Ruiz A, Berta-Thompson JW, Becker JW, Van Der Donk WA, Chisholm SW. Evolutionary radiation of lanthipeptides in marine cyanobacteria. Proc Natl Acad Sci U S A. 2017;114(27):E5424–33.
47. Li B, Sher D, Kelly L, Shi Y, Huang K, Knerr PJ, et al. Catalytic promiscuity in the biosynthesis of cyclic peptide secondary metabolites in planktonic marine cyanobacteria. Proc Natl Acad Sci U S A. 2010;107(23):10430–5.
48. Yelton AP, Acinas SG, Sunagawa S, Bork P, Pedrós-Alió C, Chisholm SW. Global genetic capacity for mixotrophy in marine picocyanobacteria. ISME J. 2016;10(12):2946–57.
49. Kettler GC, Martiny AC, Huang K, Zucker J, Coleman ML, Rodrigue S, et al. Patterns and implications of gene gain and loss in the evolution of *Prochlorococcus*. PLoS Genet. 2007;3(12):2515–28.
50. Pedler BE, Aluwihare LI, Azam F. Single bacterial strain capable of significant contribution to carbon cycling in the surface ocean. Proc Natl Acad Sci U S A. 2014;111(20):7202–7.
51. LR Moore, G Rocap, SW Chisholm. Physiology and molecular phylogeny of coexisting Prochlorococcus ecotypes. Nature. 1998;393(0):464–7.
52. Hackl T, Laurenceau R, Ankenbrand MJ, Bliem C, Cariani Z, Thomas E, et al. Novel Integrative Elements and Genomic Plasticity in Ocean Ecosystems. SSRN Electron J. 2021;
53. Shoemaker WR, Jones SE, Muscarella ME, Behringer MG, Lehmkuhl BK, Lennon JT. Microbial population dynamics and evolutionary outcomes under extreme energy limitation. Proc Natl Acad Sci U S A. 2021;118(33):1–8.
54. Brouwer AF, Eisenberg MC, Remais J V., Collender PA, Meza R, Eisenberg JNS. Modeling Biphasic Environmental Decay of Pathogens and Implications for Risk Analysis. Environ Sci Technol. 2017;51(4):2186–96.
55. Crane SR, Moore JA. Modeling enteric bacterial die-off: A review. Water, Air, Soil Pollut. 1986;27(3–4):411–39.
56. Finkel SE, Kolter R. Evolution of microbial diversity during prolonged starvation. Proc Natl Acad Sci U S A. 1999;96(7):4023–7.
57. Patra P, Klumpp S. Population Dynamics of Bacterial Persistence. PLoS One. 2013;8(5).
58. Pruitt KM, Kamau DN. Mathematical models of bacterial growth, inhibition and death under combined stress conditions. J Ind Microbiol. 1993;12(3–5):221–31.
59. Van Boekel MAJS. On the use of the Weibull model to describe thermal inactivation of microbial vegetative cells. Int J Food Microbiol. 2002;74(1–2):139–59.
60. Aguilo-Ferretjans M del M, Bosch R, Puxty RJ, Latva M, Zadjelovic V, Chhun A, et al. Pili allow dominant marine cyanobacteria to avoid sinking and evade predation. Nat Commun [Internet]. 2021;12(1):1–10. Available from: http://dx.doi.org/10.1038/s41467-021-22152-w
61. Hood RD, Higgins SA, Flamholz A, Nichols RJ, Savage DF. The stringent response regulates adaptation to darkness in the cyanobacterium *Synechococcus elongatus*. Proc Natl Acad Sci U S A. 2016;113(33):E4867–76.
62. Bergkessel M, Basta DW, Newman DK. The physiology of growth arrest: Uniting molecular and environmental microbiology. Nat Rev Microbiol. 2016;14(9):549–62.
63. Finkel SE. Long-term survival during stationary phase: evolution and the GASP phenotype. Nat Rev Microbiol [Internet]. 2006;4(2):113–20. Available from: https://doi.org/10.1038/nrmicro1340
64. Koch H, Dürwald A, Schweder T, Noriega-Ortega B, Vidal-Melgosa S, Hehemann JH, et al.

610 Biphasic cellular adaptations and ecological implications of *Alteromonas macleodii*
611 degrading a mixture of algal polysaccharides. ISME J [Internet]. 2019;13(1):92–103.
612 Available from: http://dx.doi.org/10.1038/s41396-018-0252-4
613 65. Forchielli E, Sher D, Segrè D. Metabolic phenotyping of marine heterotrophs on
614 refactored media reveals diverse metabolic adaptations and lifestyle strategies. bioRxiv
615 [Internet]. 2022;2022.01.07.475430. Available from:
616 https://www.biorxiv.org/content/10.1101/2022.01.07.475430v2%0Ahttps://www.biorxi
617 v.org/content/10.1101/2022.01.07.475430v2.abstract%0Ahttp://biorxiv.org/content/ear
618 ly/2022/01/09/2022.01.07.475430.abstract
619 66. Teeling H, Fuchs BM, Becher D, Klockow C, Gardebrecht A, Bennke CM, et al. Substrate-
620 controlled succession of marine bacterioplankton populations induced by a
621 phytoplankton bloom. Science (80-). 2012;336(6081):608–11.
622 67. Becker JW, Berube PM, Follett CL, Waterbury JB, Chisholm SW, DeLong EF, et al. Closely
623 related phytoplankton species produce similar suites of dissolved organic matter. Front
624 Microbiol. 2014;5(MAR):1–14.
625 68. Domínguez-Martín MA, López-Lozano A, Clavería-Gimeno R, Velázquez-Campoy A, Seidel
626 G, Burkovski A, et al. Differential NtcA responsiveness to 2-oxoglutarate underlies the
627 diversity of C/N balance regulation in *Prochlorococcus*. Front Microbiol. 2018;8(JAN):1–
628 16.
629 69. Reich T, Ben-Ezra T, Belkin N, Tsemel A, Aharonovich D, Roth-Rosenberg D, et al. A year in
630 the life of the Eastern Mediterranean: Monthly dynamics of phytoplankton and
631 bacterioplankton in an ultra-oligotrophic sea. Deep Res Part I Oceanogr Res Pap
632 [Internet]. 2022;182(February):103720. Available from:
633 https://doi.org/10.1016/j.dsr.2022.103720
634 70. Ma L, Calfee BC, Morris JJ, Johnson ZI, Zinser ER. Degradation of hydrogen peroxide at
635 the ocean's surface: The influence of the microbial community on the realized thermal
636 niche of *Prochlorococcus*. ISME J [Internet]. 2018;12(2):473–84. Available from:
637 http://dx.doi.org/10.1038/ismej.2017.182
638 71. Malmstrom RR, Coe A, Kettler GC, Martiny AC, Frias-Lopez J, Zinser ER, et al. Temporal
639 dynamics of *Prochlorococcus* ecotypes in the Atlantic and pacific oceans. ISME J.
640 2010;4(10):1252–64.
641 72. Beckett SJ, Demory D, Coenen AR, Casey JR, Dugenne M, Follett CL, et al. Diel population
642 dynamics and mortality of *Prochlorococcus* in the North Pacific Subtropical Gyre. 2021;1–
643 20.
644 73. Moore LR, Coe A, Zinser ER, Saito MA, Sullivan MB, Lindell D, et al. Culturing the marine
645 cyanobacterium *Prochlorococcus*. Limnol Oceanogr Methods. 2007;5(OCT):353–62.
646 74. Grossowicz M, Roth-Rosenberg D, Aharonovich D, Silverman J, Follows MJ, Sher D.
647 *Prochlorococcus* in the lab and in silico: The importance of representing exudation.
648 Limnol Oceanogr. 2017;62(2):818–35.